A Four-Bit Digital Microinjector Using Microheater Array for Adjusting the Ejected Droplet Volume

Tae Goo Kang and Young-Ho Cho, *Member, IEEE, Member, ASME*

***Abstract*—In this paper, we present the design, fabrication, and experimental results of 4-bit digital microinjectors, whose ejected droplet volumes are adjusted by the digital operation of a 4-bit microheater array. We design the reference microinjectors as well as its comparative test structures. In the fabrication process, we use a five-mask micromachining process and the total chip size of the fabricated microinjector is 7640 μm$\times$ 5260 μm. We observe the microbubble generation and collapse on the microheater array. The microbubbles initiate and grow individually on top of each operating microheater, however the microbubbles merge together before collapse. We measure the ejected droplet volumes and velocities, which are adjusted from 12.1 ~ 55.6 pl and 2.3 ~ 15.7 m/s, respectively, depending on the 15 possible combinations of 4-bit microheater array. We also experimentally characterize the effect of geometric variation including the microheater size, intermicroheater gap, microchannel width and sequential operation of microheater array on the ejected droplet volume and velocity. Thus, the present microinjector has a potential for application to the high-resolution inkjet printers with multiple gray levels or high-precision fluid injectors with variable volume control. [1348]**

***Index Terms*—Droplet volume adjusting, inkjet printer, microheater array, microinjector.**

I. Introduction

MICRODROPLET injectors have been widely developed for the application to the inkjet printheads [1], [2], fuel injection systems [3], drug delivery systems, direct print lithography, and micro jet propulsion systems. Among those applications of microinjectors, inkjet printhead has been developed by major companies such as HP, Canon, Xerox, *et al.*, due to the huge market of desktop printer application. Nowadays, with the rapid growth of the Internet and digital photography, there is great demand for a cheap method to print colored images and photographs.

There are two key factors for the low-cost printing of colored images using the inkjet printers: the printing resolution (or image quality) and the printing speed. However, there is a tradeoff between these two. When the resolution is doubled, 4 times more droplets are required to cover the same area and hence the printing speed is decreased by a factor of 4 times. From this point of view, a droplet volume adjustable printing technology is attractive due to its potential to improve or optimize the printing speed [4], [5] of high-quality colored images. There are some previous works for adjusting the droplet volumes: using a multiple pulse packet [6]; dual nozzle microinjector [7]; and dual heater microinjector with different size [8]. The advantage of the first one is its simple structure, but it has a limited adjustment range. The second one needs twice as many nozzles. The third one has complex operating electrical signals due to the different sizes of its two microheaters.

In this work, we present a 4-bit digital microinjector using a microheater array to adjust the ejected droplet volume. This microinjector can generate multilevel droplet volume with a wide range by digitally controlling microheaters with an identical electrical operating signal. We experimentally characterize the effect of heater size, intermicroheater gap, microchannel width, and sequential operation of microheater array on the ejected droplet volume and the velocity of the microinjectors.

Manuscript received May 24, 2004; revised March 21, 2005. This work has been supported by the National Creative Research Initiative Program of the Ministry of Science and Technology (MOST) under the project title of "Realization of Bio-Inspired Digital Nanoactuators." Subject Editor C. Liu.

The authors are with the Digital Nanolocomotion Center, Korea Advanced Institute of Science and Technology, Daejeon 305-701, Republic of Korea (e-mail: nanosys@kaist.ac.kr).

Digital Object Identifier 10.1109/JMEMS.2005.851864

II. Theoretical Analysis

A. Working Principle of the 4-Bit Digital Microinjector

Fig. 1 shows the structure of the droplet volume adjustable microinjector, which has a 4-bit digital microheater array. Fig. 2 illustrates the digital operation of the 4-bit microheater array: For the digital turn-on of the microheater, b_1, the smallest microbubble is generated on the microheater [see Fig. 2(a)], thus ejecting the minimum amount of fluid volume through the nozzle; For the digital turn-on of the multiple microheaters, b_1, b_2 and b_3, the larger microbubble [see Fig. 2(b)] ejects the larger amount of fluid volume.

B. Theoretical Analysis

In the theoretical analysis, we have modified the previous theoretical model [9], [10] of bubble growth and liquid flow in the single microheater bubble jet printhead. The operation cycle of a bubble jet is divided into three phases: Phase 1—heating ink until a vapor bubble is generated; Phase 2—bubble growth and collapse with droplet formation; Phase 3—refill of ink by surface tension.

In phase 1, heat is conducted from a resistor to the ink and substrate. In this work, we treat the heat transfer process as one-dimensional heat conduction [9], [10], since the thickness of the heater and the distance to which heat is conducted during a heating period (~ 1 μsec) is small compared with the size of the heating area. The heat generation rate [9] per unit volume and unit time period at the resistor is given by

$$q^{\cdot} = \left(\frac{V_{op}^2}{R_H}\right)\frac{1}{S_H d_H} \tag{1}$$

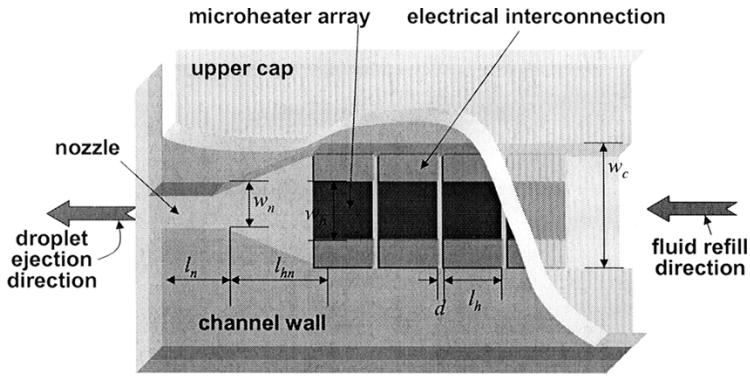

Fig. 1. Structure of the multilevel microfluid injector.

where V_{op} is the operating voltage, R_H is the resistance of the resistor, S_H is the heating area of the resistor and d_H is the thickness of the resistor. Isothermal boundary conditions are used at the top of the ink layer and the bottom of the substrate before the boiling.

In normal boiling situation, liquids begin to boil at their boiling points. However, in a inkjet device, vapor bubbles are generated at a temperature far above the normal boiling point of ink [9], [10]. For typical operating conditions with water, the estimated value of the bubble generation temperature [8], $T_{\rm gen}$, is about 270 °C. When the surface temperature of microheater reaches $T_{\rm gen}$, we stop to solve the heat conduction equation and replace the boundary condition to the adiabatic condition at the top surface of the microheater due to the thermal insulation of generated microbubble. Additionally, we turn off the electrical input signal at which the surface temperature of microheater reaches $T_{\rm gen}$. Thus, the temperature of the microheater starts to decrease. With the replaced boundary condition, we can estimate the temperatures of microheater surface at time t.

The next step is to predict the bubble pressure. The temperature, T_v, and pressure, P_v, in the bubble are assumed to be uniform and are related by an integral form of the equilibrium Clapeyron-Clausius equation [9]:

$$P_v = P_{\rm atm} \exp\left[\frac{wQ_{\rm vap}}{R}\left(\frac{1}{T_b} - \frac{1}{T_v}\right)\right] \tag{2}$$

where $P_{\rm atm}$ is the atmospheric pressure ($= 101.3\,{\rm kPa}$), R is the gas constant ($= 8.3148\,{\rm J/mol{\cdot}K}$), T_b is the boiling point of ink, and w, $Q_{\rm vap}$ and ρ_v are molecular weight, heat of vaporization and density of vapor, respectively. For water, the properties at its boiling point are used: $T_b = 100°{\rm C}$, $w = 18 \times 10^{-3}\,{\rm kg/mol}$ and $Q_{\rm vap} = 2.26 \times 10^6\,{\rm J/kg}$.

We convert the bubble pressure into the equivalent channel cross-section pressure. With the assumption of no viscous friction, we can estimate the channel cross-section pressure at the end point of the microheater as follows:

$$P_c = \frac{1}{2}\frac{A_b}{A_c}P_v \tag{3}$$

where the P_c is the channel cross-section pressure, and A_b and A_c are the area of microbubble (the area of the microbubble is assumed to be the same as the area of the operating microheaters) and the channel cross-section, respectively.

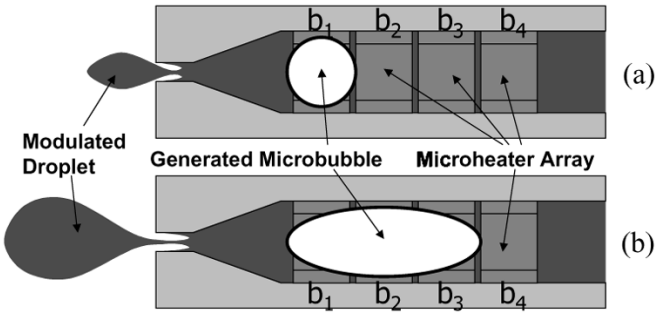

Fig. 2. Digital operation of the 4-bit digital microheater array in the microinjector of Fig. 1: (a) the operation mode of $(b_1, b_2, b_3, b_4) = (1, 0, 0, 0)$ and (b) the operation mode of $(b_1, b_2, b_3, b_4) = (1, 1, 1, 0)$.

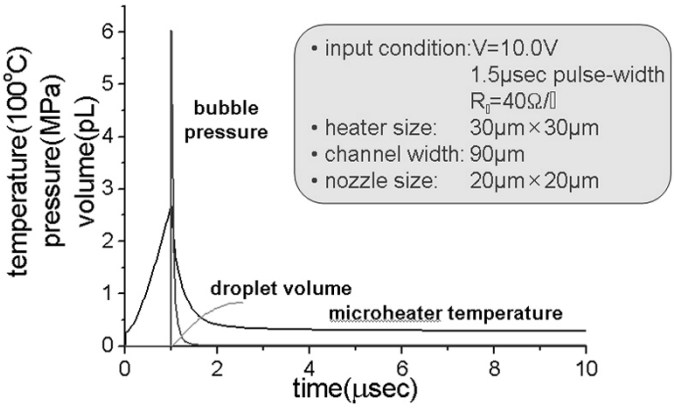

Fig. 3. Theoretical estimation of the microheater temperature, the bubble pressure, and the droplet volume for the operation mode of (1000).

TABLE I
DIMENSIONS OF THE DESIGNED MICROINEJCTOR IN FIG. 1

Microheater Size (l_h×w_h×t_h)	40μm×40μm×100nm
Inter-Microheater Gap	3μm
Channel Width (w_c)	60μm
Channel Length (l_c)	250μm
Channel and Nozzle Depth	30μm
Converging Channel Length (l_{hn})	50μm
Nozzle Length (l_n)	30μm
Nozzle Width (w_n)	30μm

TABLE II
DESIGN VARIATIONS OF COMPARATIVE TEST STRUCTURES

Test Structures	Heater Size, ($l_h \times w_h$)	Test Structures	Inter-Microheater Gap (d)	Test Structures	Channel Width (w_c)
H1	30μm×30μm	G1	5μm	W1	80μm
H2	50μm×50μm	G2	10μm	W2	100μm

All Dimensions unless specified are identical with the dimensions of reference test structure in Table I.

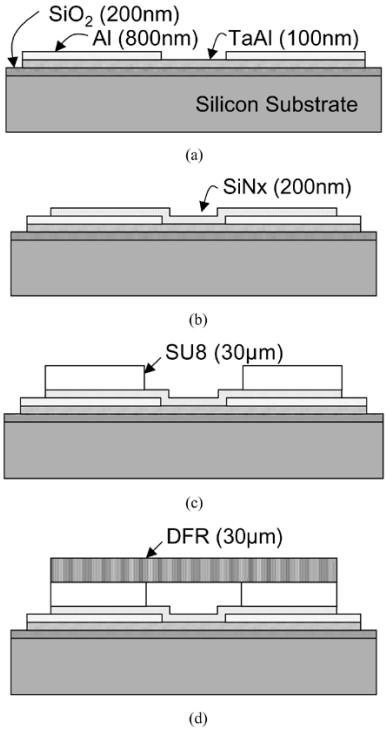

Fig. 4. Fabrication process for the microinjector.

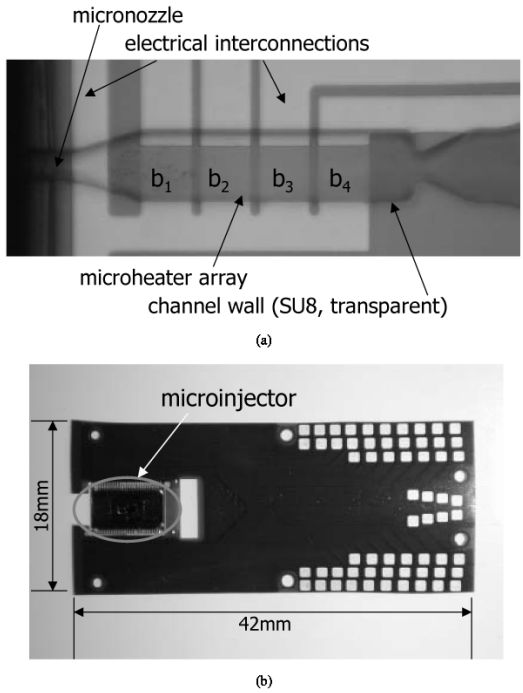

Fig. 5. Photographs of the fabricated devices: (a) microheater array and micronozzle and (b) microinjector attached to Flexible Printed Circuit (FPC).

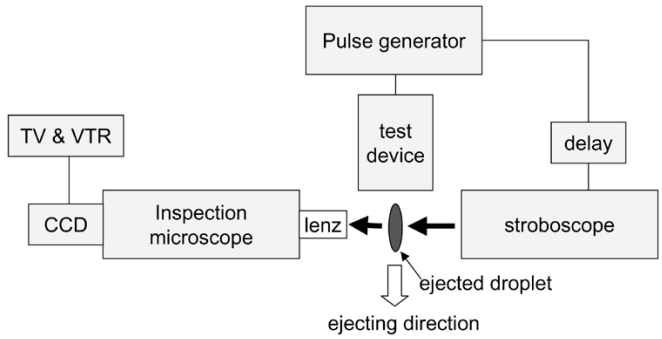

Fig. 6. Experimental apparatus for microinjector characterization.

We estimate the ejected microdroplet volume using the following equation [11]:

$$\rho A \frac{d^2V}{dt^2} + \eta B \frac{dV}{dt} = P_c - P_{\text{atm}} \tag{4}$$

where ρ, η and V are the density, the viscosity and the droplet volume. In (4), the inertance factor, A, and the resistance factor, B, of a square pipe of length, l, with the width, $a(x)$, and the height, $b(x)$, are given [11] by

$$A = \int_0^l \frac{1}{a(x)b(x)} dx \tag{5}$$

$$B = \int_0^l \frac{G(x)}{\{a(x)b(x)\}^2} dx \tag{6}$$

where $G(x)$ is approximately given by

$$G(x) \approx 12 \left[0.33 + 1.02 \left\{ \frac{a(x)}{b(x)} + \frac{b(x)}{a(x)} \right\} \right]. \tag{7}$$

The compressibility of the water and the surface tension at the liquid-vapor interface and liquid-air interface are neglected in this model.

C. Design

On the basis of the theoretical analysis, we designed the 4-bit digital microinjector (reference test structure, R), whose dimensions are listed in the Table I. For the reference test structure, we have estimated the microheater temperature, the microbubble pressure, as well as the ejected fluid volume. Results for the (1000) mode are shown in Fig. 3. We also designed the comparative test structures having variation of the microheater size from 30 μm to 50 μm, the inter-microheater gap from 3 μm to 10 μm, and the microchannel width from 60 μm to 100 μm (Table II) in

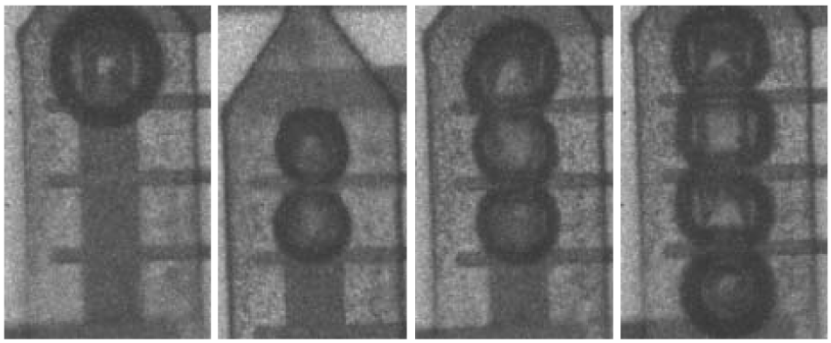

Fig. 7. The maximum bubble sizes observed at 2 μs after the microheater turn-on using 1 kHz, 1.5 μsec, 10 V pulse signals for the different operation modes: (a) (1000) mode; (b) (1100) mode; (c) (1110) mode; (d) (1111) mode.

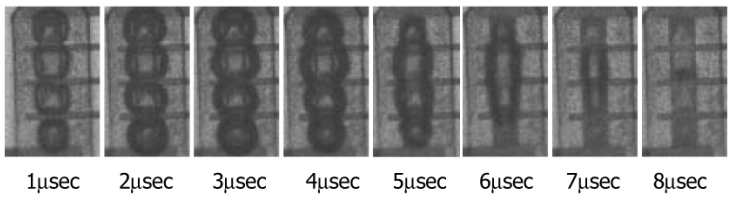

Fig. 8. Measured life-history of the generated microbubble having the time sequence of 1 μs after a 10.0 V, 1 kHz, 1.5 μs pulsewidth electrical input signal is applied for the case of (1111) operation.

order to experimentally characterize the effect of the design parameters and operating conditions on the ejected droplet volume and velocity.

III. Fabrication Process

The five-mask fabrication process for the microinjector is illustrated in Fig. 4. First, a 100-nm-thick TaAl layer is patterned for the microheater fabrication and a 800 nm-thick Al layer is used for the electrical interconnections [see Fig. 4(a)]. The measured sheet resistance of TaAl resistor is $30 \pm 0.3\ \Omega$. We choose the TaAl thin layer [3] as the heater material because of its high resistivity, high melting point and small heat capacity. In addition, TaAl is a mechanically strong and noncorrosive material in acid atmosphere. A silicon nitride insulation layer is deposited and patterned over the aluminum [see Fig. 4(b)]. After that, the 30-μm-thick SU8 2025 forms the microchannel barrier and nozzle layer [see Fig. 4(c)] and the 30 μm-thick DFR (Dry Film PhotoResist, KG-5100), laminated on the SU8 layer [see Fig. 4(d)], serves as the top-layer. Fig. 5(a) shows the fabricated unit microinjector and Fig. 5(b) shows the fabricated device, attached to FPC (Flexible Printed Circuit) for performance characterization. The total size of fabricated microinjector chip is 7640 μm$\times$ 5260 μm.

IV. Experimental Results and Discussions

Fig. 6 shows the experimental apparatus for measuring the volume and velocity of the ejected fluid. The microheaters have identical turn-on electrical signals of 1 kHz, 1.5 μs, 10 V square pulse. In order to take pictures of generated microbubbles and the ejected droplets, we use a CCD camera and a stroboscope, which were synchronized with the input electrical pulse generator. The frames shown in Figs. 7–10 are overlapped image

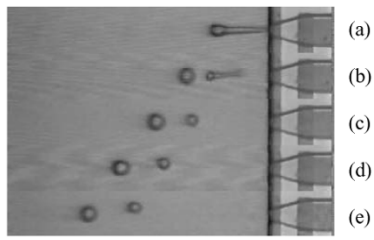

Fig. 9. Trajectory of the ejected fluid for the operation mode of (1000): The images are taken at (a) 10 μs; (b) 20 μs; (c) 30 μs; (d) 40 μs; (e) 50 μs after the microheater turn-on.

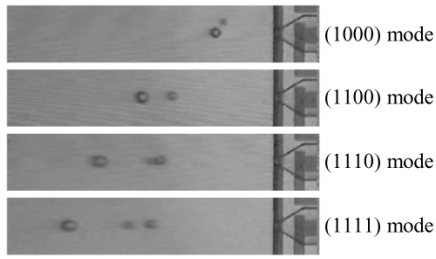

Fig. 10. Trajectories of the ejected fluid at the 50 μs after turn on for the operation mode of (1000), (1100), (1110), and (1111), respectively.

of 30 to 40 pictures, taken at the same moment in their operating period. The uniformity and consistency of the overlapped bubbles (Figs. 7 and 8) and droplets (Figs. 9 and 10) show the uniformity and repeatability of the experiments. We extracted the measured data of droplet volumes and velocities, using the picture captured from a single frame of the CCD camera. For example, we extract the droplet volume from the diameter of the ejected droplet, and the velocity from the distance between the nozzle exit and the ejected droplet at a specific time frame. In this paper, we consider the droplet volumes and velocities from the main droplet neglecting the satellite droplets.

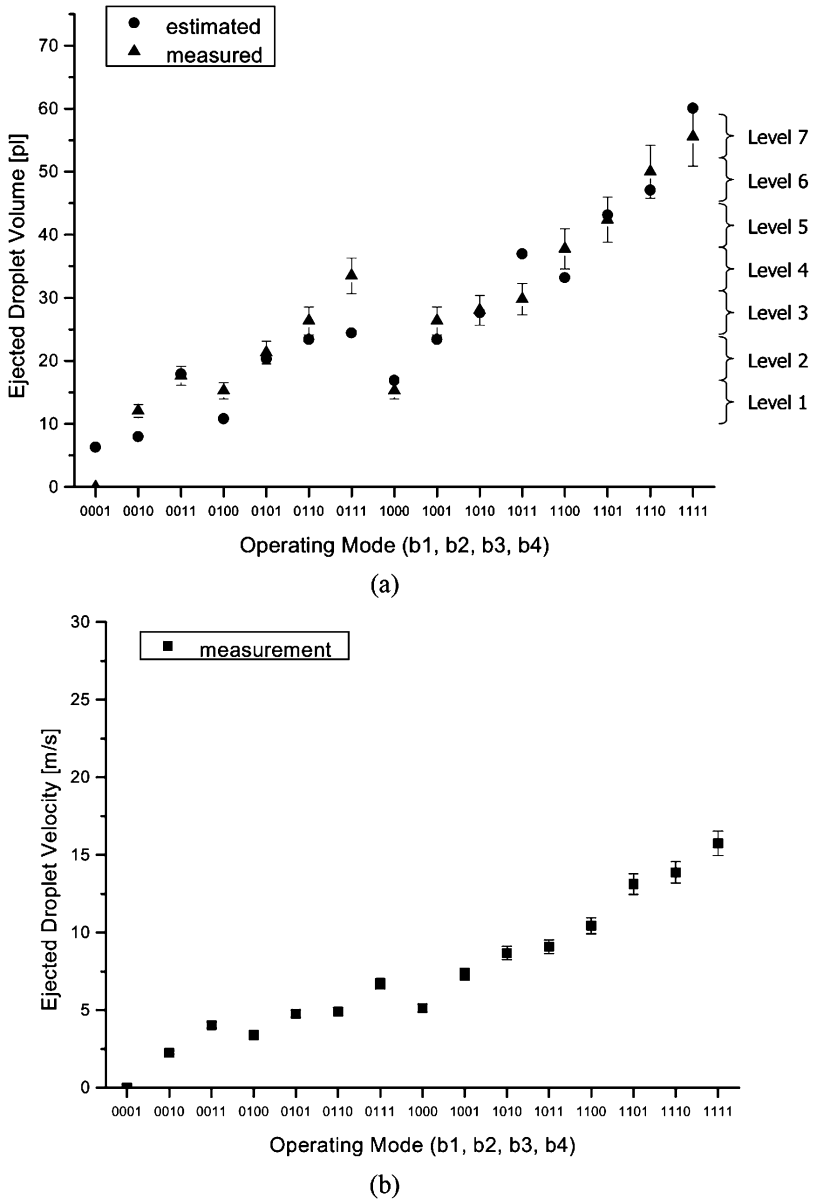

Fig. 11. The measured volume and velocity of the fluid, ejected for 15 possible combinations of the 4-bit digital operation mode: (a) volume and (b) velocity.

A. Bubble Generation, Growth, and Collapse

Fig. 7 shows the maximum size of microbubbles for the 4-bit operation of the 30±2Ω-microheater array at 2 μs after turn-on. The bubble collapse time, however, depends on the operation mode: (1000) operation mode shows the shortest collapse time of 4 μs, while (1111) operation mode shows the longest time of 8 μs (see Fig. 8). The reason is that bubbles start to grow separately on each microheater to their maximum size, at which point they merge into a single larger bubble before collapsing. Thus, a longer collapse time is needed for the larger bubble.

B. Digital Operation of 4-Bit Microheater Array

Fig. 9 shows an example of the fluid ejection trajectory, taken for the operation mode of (1000) at the time interval of 10 μs after the microheater turn-on. Fig. 10 shows the ejected trajectories at 50 μs after the microheater turn-on for each operation modes. From the fluid ejection trajectory taken for 15 possible combination cases of 4-bit digital operation mode, the droplet volumes and velocities are measured in the ranges of 12.1 ± 1.0~55.6 ± 4.7 pl [see Fig. 11(a)] and 2.3 ± 0.1~15.7 ± 0.8 m/s [see Fig. 11(b)], respectively (the result of (0001) mode is not included because no droplet is ejected). Also we find that the theoretical estimation of the ejected droplet volume shows quite good agreement with the experimental estimations to predict its tendency with respect to the operation mode. From Fig. 11(a), we find that 15 digital operation modes produce seven distinguishable droplet volume levels on the basis of 7 pl [12] resolution.

As shown in Fig. 10, the operation mode number is not directly proportional to the droplet volume and velocity. Generally, the droplet volume and the velocity are functions of many parameters such as microheater size, channel geometry, nozzle geometry, and the input electrical signal, etc. In this

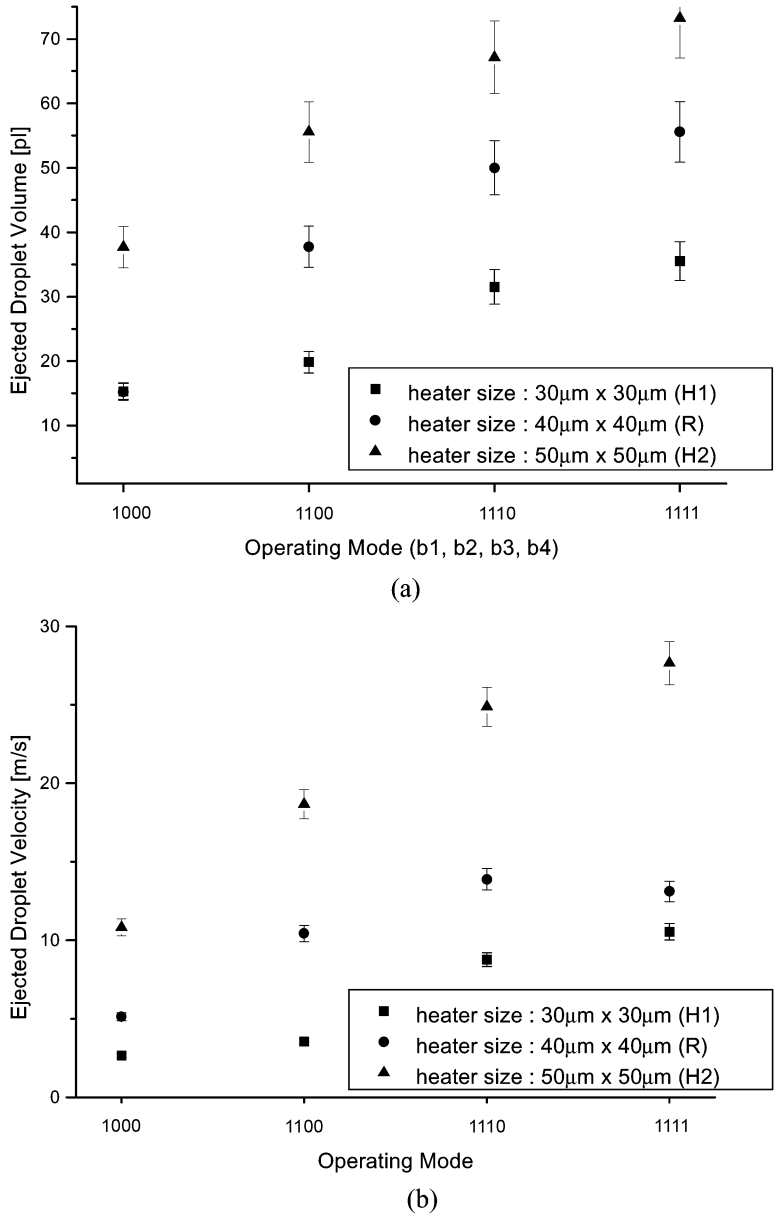

Fig. 12. Effect of the microheater size on the ejected droplet volume and velocity measured from the selected 4-bit digital operation of (1000), (1100), (1110), and (1111): (a) droplet volume and (b) droplet velocity.

work, we experimentally characterize the effects of microheater size, inter-microheater gap, the channel width, and sequential operation of the microheater array, respectively.

C. Effect of the Microheater Size (Test H)

Fig. 12 shows the measured ejected droplet volumes and velocities for microheater sizes of 30 μm $\times$ 30 μm, 40 μm $\times$ 40 μm, 50 μm $\times$ 50 μm with other geometries fixed. As shown in Fig. 12, the droplet volume as well as the droplet velocity increases as microheater size increases. The reason is that the microheater size is proportional to the channel pressure (3), which is the input pressure of the droplet formation. For example, the ratio of area variation ($30\,\mu\text{m}\times30\,\mu\text{m}$:$40\,\mu\text{m}\times40\,\mu\text{m}$:$50\,\mu\text{m}\times50\,\mu\text{m}$= 1:1.78:2.78) causes the ratio of ejected droplet volume (35.5 pl:55.6 pl:73.2 pl = 1:1.57:2.06 for the case of (1111) operation mode).

D. Effect of the Intermicroheater Gap (Test G)

Fig. 13 shows the measured ejected droplet volumes and velocities for inter-microheater gaps of 3 μm, 5 μm, 10 μm with other geometries fixed. As shown in Fig. 13, the droplet volume decreases but velocity increases as the inter-microheater gap increases.

E. Effect of the Microchannel Width (Test W)

Fig. 14 shows the measured ejected droplet volumes and velocities for microchannel widths of 60 μm, 80 μm, 100 μm with other geometries fixed. As shown in Fig. 14, the droplet volume and velocity decrease as the microchannel width increases. The reason for the ejected droplet volume decrease is that the channel pressure (3) is inversely proportional to the channel cross-section area. However, microchannel width affects to the hydrodynamic channel inertance and resistance

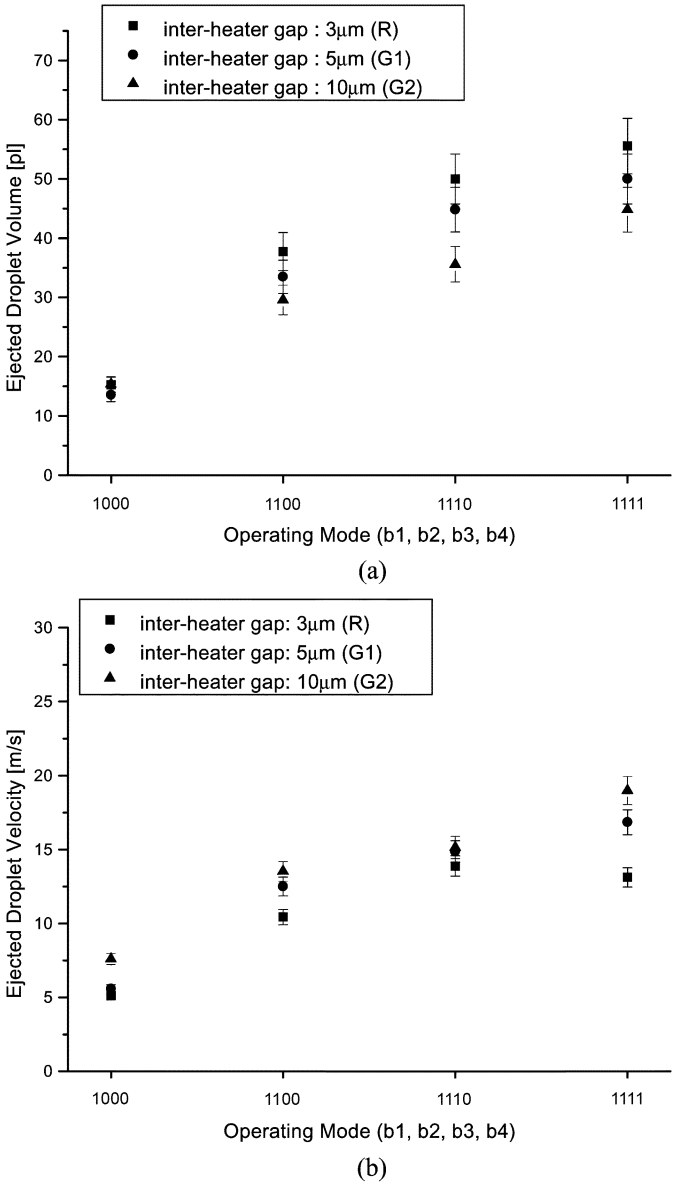

Fig. 13. Effect of the inter-microheater gap on the ejected droplet volume and velocity measured from the selected 4-bit digital operation of (1000), (1100), (1110), and (1111): (a) droplet volume and (b) droplet velocity.

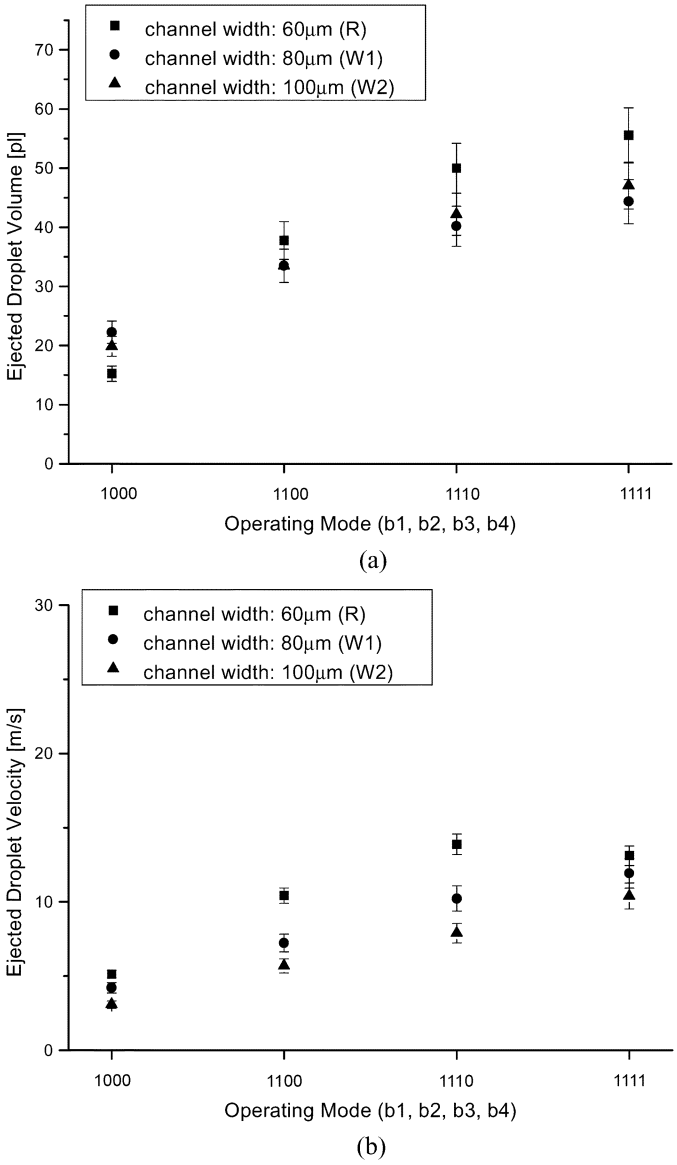

Fig. 14. Effect of the microchannel width on the ejected droplet volume and velocity measured from the selected 4-bit digital operation of (1000), (1100), (1110), and (1111): (a) droplet volume and (b) droplet velocity.

(4), which decrease as microchannel width increase. This is the reason why some operation modes show inverse characteristics as stated above.

F. Effect of the Sequential Operation of Microheater Array (Test S)

Fig. 15 shows the measured ejected droplet volumes and velocities for varying firing times of each operating microheater, delayed by 0, 1.3, 2.3, 3.4 μs from farthest microheater to nearest microheater from nozzle exit. As shown in Fig. 15, the droplet volumes and velocities decrease as the delay time increases. The reason, we think, is due to the occurrence of microflow interference in the microchannel caused by sequentially turning on/off the microheater.

V. Conclusion

In this paper, we presented a droplet volume adjustable thermofluidic digital microinjector using 4-bit digital microheater array. In the theoretical analysis, we estimated microheater temperature, bubble pressure and droplet volume of the microinjector. In the experimental study, we observed that the maximum size of generated microbubble occurs at 2 μs after turn-on, and the collapse time of the bubble is depends on the operation mode of the microheater array. We also measured ejected droplet volumes in the range of 12.1 $\pm$ 1.0 ~ 55.6 $\pm$ 4.7 pl and ejected droplet velocities in the range of 2.3 $\pm$ 0.1 ~ 15.7 $\pm$ 0.8 m/s depending on the 15 possible operation modes of 4-bit digital microheater array. Also, we experimentally characterized the effect of the microheater size, inter-microheater gap, microchannel width and the sequential operation of microheater array on the ejected droplet volumes and velocities. Con-

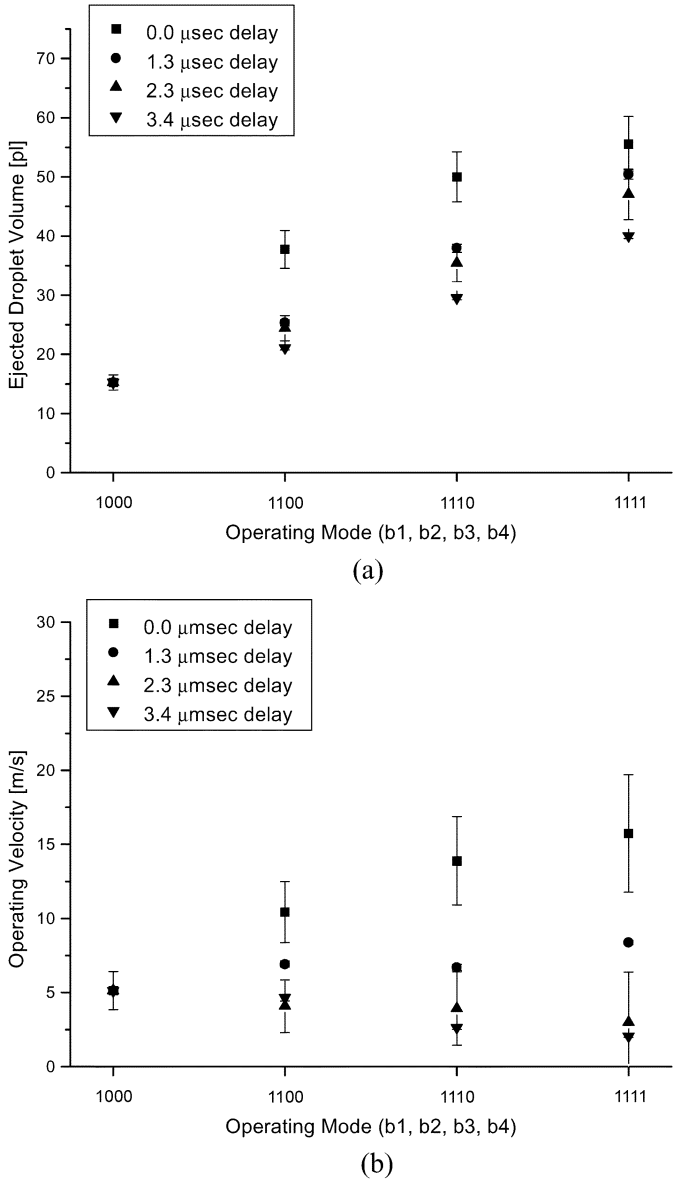

Fig. 15. Effect of the sequential operation of the microheater array on the ejected droplet volume and velocity measured from the selected 4-bit digital operation of (1000), (1100), (1110), and (1111) for the test structure of R: (a) droplet volume and (b) droplet velocity.

sequently, the present droplet volume adjustable microinjectors have the potential to optimize the printing speed as well as the image quality of high-resolution inkjet printers.

REFERENCES

[1] R. N. Mills, "Ink jet printing—Past, present and future," in *Proc. IS&T's Tenth International Congress on Advanced in Non-Impact Printing Technologies*, New Orleans, LA, 1994.

[2] S. Pond, "Drop-on-Demand ink jet transducer effectiveness," in *Proc. IS&T's Tenth International Congress on Advanced in Non-Impact Printing Technologies*, New Orleans, LA, 1994.

[3] F. G. Tseng, C. J. Kim, and C. M. Ho, "A microinjector free of satellite drops and characterization of the ejected droplets," in *Proc. ASME*, Anaheim, CA, Nov. 1998, pp. 89–96.

[4] J. P. Stefanini, "Automated print quality optimization apparatus," in *Proc. 7th Annual European Ink Jet Printing Conference*, Barcelona, Spain, 1999.

[5] R. N. Mills, "Ink jet printing in a competitive marketplace," in *Proc. 7th Annual European Ink Jet Printing Conference*, Barcelona, Spain, 1999.

[6] A. T. Christopher, "Method and Apparatus for Generating a Gray Scale With a High Speed Thermal Ink Jet Printer," U.S. Patent no. 4 503 444, 1985.

[7] F. E. Anderson, J. P. Bolash, R. W. Cornell, and G. K. Parish, "Dual Droplet Size Printhead," U.S. Patent no. 6 137 502, 2000.

[8] H. Ishinaga, M. Ikeda, T. Abe, and T. Kashino, "Method for Ink-Jet Recording and an Ink-Jet Recording Apparatus," U.S. Patent no. 6 142 599, 2000.

[9] A. Asai, T. Hara, and I. Endo, "One-Dimensional model of bubble growth and liquid flow in bubble jet printers," *Jpn. J. Appl. Phys.*, vol. 26, no. 10, pp. 1794–1801, 1987.

[10] P.-H. Chen, W.-C. Chen, and S.-H. Chang, "Bubble growth and ink ejection process of a thermal ink jet printhead," *Int. J.Mechan. Sci.*, vol. 39, no. 6, pp. 683–695, 1997.

[11] J. D. Beasley, "Model for fluid ejection and refill in an impulse drive jet," *Photograph. Sci. Eng.*, vol. 21, pp. 78–82, 1977.

[12] M. Wills, "Ink jet printing technology for the next millenium," in *Proc. 7th Annual European Ink Jet Printing Conference*, Barcelona, Spain, 1999.

Tae Goo Kang was born in Daegu, Korea, in 1972. He received the B.S. and M.S. degrees from the Department of Mechanical Engineering at the Korea Advanced Institute of Science and Technology (KAIST), Seoul, in 1994 and 1997, respectively. His research interests are focused on microfluidic systems and BioMEMS. Currently, he is working on microinjectors for his Ph.D at KAIST.

Since 2000, he has been working at Digital Nanolocomotion Center (DNC) as a Research Engineer.

Young-Ho Cho (M'02) received the B.S. degree (*summa cum laude*) from Yeungnam University, Daegu, Korea, in 1980, the M.S. degree from the Korea Advanced Institute of Science and Technology (KAIST), Seoul, in 1982, and the Ph.D. degree from the University of California at Berkeley for his electrostatic actuator and crab-leg microflexure research completed in December 1990.

From 1982 to 1986, he was a Research Scientist of CAD/CAM Research Laboratory, Korea Institute of Science and Technology (KIST), Seoul, Korea. During 1987–1991, he worked as a Postgraduate Researcher (1987–1990) and a Postdoctoral Research Associate (1991) of the Berkeley Sensor and Actuator Center (BSAC) at the University of California at Berkeley. In August 1991, Dr. Cho moved to KAIST, where he is currently an Associate Professor in the Departments of BioSystems & Mechanical Engineering as well as the Director of Digital Nanolocomotion Center. His research interests are focused on the optomechanical and biofluidic MEMS with micro/nano-scaled actuators and detectors for photon manipulation and biomedia processing.

Dr. Cho's has served, in Korea, as the Chair of MEMS Division in Korean Society of Mechanical Engineers, the Chair of Steering Committee in Korea National MEMS Programs, the Chair of Steering Committee in Korean Next Generation Technology Development Program, the Leader of Nanobio-Group in National NanoForum and the Committee of National Nanotechnology Planning Board. He has also served for international technical society as the General Co-Chair of IEEE MEMS Conference 2003, the Program Committee of IEEE Optical MEMS Conference, and the Chief Delegate of the Republic of Korea in World Micromachine Summit. He is a member of the American Society of Mechanical Engineers (ASME).